  Bull. Chem. Soc. Jpn., 62, 1715—1724 (1989)

Direct Determination of Hyperfine Coupling Constants from Complex and Poorly Resolved ESR Spectra with Numerical Decoupling Analysis

Koichi Nozaki, Akira Naito, Hiroyuki Hatano, and Satoshi Okazaki*
Department of Chemistry, Faculty of Science, Kyoto University, Sakyo-ku, Kyoto 606
(Received November 4, 1988)

Numerical decoupling analysis (NDA) has been developed as a useful analytical method for determining accurate hyperfine coupling constants (hfccs) involved in isotropic ESR spectra with constant linewidths. NDA was found to have a number of advantages over other methods developed for the extraction of hfccs from ESR spectra. For example, the nuclear spin (e.g., I=1/2 or 1) can easily be distinguished and hfccs as small as a linewidth can be determined. Furthermore, false hfccs which often appear and lead to confusion in obtaining the true values in other methods are largely eliminated. Owing to these advantages NDA has enabled us to interpret not only complex but also poorly resolved ESR spectra. The practical use of NDA could be demonstrated by analyzing the ESR spectra of *t*-butyl 4-nitrophenyl nitroxide and *t*-butyl 2-chlorophenyl nitroxide radicals.

While a computer simulation method has usually been used as a suitable means of interpreting complicated ESR spectra, it is tedious to determine the ESR parameters with increasing numbers. Furthermore, when an ESR spectrum is poorly resolved it is rather difficult to accurately determine the parameters. Thus, in any case, some degree of experience is required to analyze such an ESR spectrum.

In order to help with the computer simulation analysis of ESR spectra various useful techniques have been reported. For an automatic improvement in the initially estimated set of parameters, a large number of curve-fitting methods are available.[1-4] Most of them employ nonlinear least-squares techniques which generally require a finely tuned data set as the initial parameters. Without such parameters they may not converge or be trapped in an undesirable local minimum of the error function. However, new methods using Simplex[5] or Monte Carlo[6] techniques have proven to be very reliable, especially in systems involving many parameters since they enable one to search for the minimum globally.

On the other hand, if accurate parameters can be independently determined from the hyperfine structure (hfs) of an observed ESR spectrum, one could readily interpret the ESR spectrum without relying on any experience or prejudices, which sometimes cause incorrect interpretations. For this purpose, an autocorrelation method[7-10] as well as Cepstral[11] and Fourier analyses[12,13] have been applied. More recently, Dračka obtained proton and nitrogen hfccs from a complex ESR spectrum by using a 'contraction' method.[14] Motten introduced a simple method using a concept similar to those of Dračka and Newton[15] in order to extract proton hfccs.[16] Lüders determined the hfcc as small as a linewidth by means of a symmetry development transformation.[17] It is, however, still difficult to obtain parameters from poorly resolved and complex ESR spectra, since most of these methods suffer from the appearance of false hfcc peaks, such as ghosts[11,17] or odd harmonics,[15,16] and some methods can only be applied to well-resolved ESR spectra.[14]

Numerical decoupling analysis (NDA), as described in this paper, has been developed as a convenient method to determine hfccs from poorly resolved and complex ESR spectra. The basic principle of NDA involves a search for hfccs by trial and error using a micro-computer. The procedure contains two steps. The first step is a trial to remove the splittings of a given value using the least-squares method. We call this procedure 'numerical decoupling'. The second step involves an evaluation of the results of the numerical decoupling using a specific index function, ascertaining whether the value is one of the hfccs.

NDA possesses some advantages over the other methods. For example, NDA enables one to determine hfccs as small as a linewidth and to distinguish the nuclear spin. Moreover, false hfccs, which sometimes disturb the determination of the hfccs, were largely discriminated.

This paper describes the theory of NDA and its practical applications to several systems.

Theory

Numerical Decoupling Analysis for Nuclei with I=1/2. When one nucleus with nuclear spin, I, of 1/2 and a hfcc of **a** contributes to an isotropic ESR spectrum with a constant linewidth, $R(\omega)$, it can be represented by the following form:

$$R(\omega)=F(\omega+\mathbf{a}/2)+F(\omega-\mathbf{a}/2), \quad (1)$$

where $F(\omega)$ is the ESR spectrum without the contribution of this nucleus. We call it a *sub-spectrum*. Furthermore, at least some of the x values at which $R(\omega)$ can be written in the same form as Eq. 1 must be the hfccs involved in $R(\omega)$:

$$R(\omega)=S(\omega+x/2)+S(\omega-x/2). \quad (2)$$

Here $S(\omega)$ is a certain function.

First, these x values are obtained through the following procedures. An error function, $d(x)$ is defined by

$$d(x)\equiv\int_{-\infty}^{\infty}[R(\omega)-S(\omega+x/2)-S(\omega-x/2)]^2\,d\omega, \quad (3)$$

where $R(\omega)$ is an observed ESR spectrum. Actually, $R(\omega)$ is represented by a series of data sampled under a magnetic field that is increasing with a constant increment. Thus, Eq. 3 can be rewritten as Eq. 4 for numerical calculation:

$$d(x)\equiv\sum_{i=1+x/2}^{N-x/2}[R(i)-S(i+x/2)-S(i-x/2)]^2, \quad (4)$$

where N is the number of data points of $R(\omega)$ and $x/2$ must be an integer having a value between 0 and N.

According to the basic theory of the least-squares method, the following simultaneous equations are obtained under the conditions $\partial d(x)/\partial S(i)=0$ ($i=x+1,x+2,\cdots,N-x$):

$$\begin{aligned}
&S(1)+2S(1+x)+S(1+2x)=R(1+x/2)+R(1+3x/2)\\
&S(2)+2S(2+x)+S(2+2x)=R(2+x/2)+R(2+3x/2)\\
&\qquad\vdots\qquad\qquad\qquad\vdots\\
&S(N-2x)+2S(N-x)+S(N)=R(N-3x/2)+R(N-x/2).
\end{aligned} \quad (5)$$

In addition, Eq. 6 is obtained as the result of the reasonable assumption that the intensities at the far ends of the tails of an observed ESR spectrum are regarded as zero:

$$\begin{aligned}
&S(1)=S(2)=\cdots S(x)=0.0,\\
&S(N-x+1)=\cdots=S(N)=0.0.
\end{aligned} \quad (6)$$

Thus, $S(i)$, ($i=1,2,\cdots N$) and $d(x)$ can be calculated from Eqs. 5 and 4, respectively. Since the error function $d(x)$ is equal to 0 when Eq. 2 holds, one can readily determine the x value at which $d(x)$ becomes 0 in a plot of $d(x)$ against x.

Second, we considered the relationship between these x values and the hfccs. When $R(\omega)$ is represented by Eq. 1, namely, the hfcc of **a** is involved in $R(\omega)$, $d(\mathbf{a})$ is obviously equal to 0 and $S(\omega)$ is identical to the *sub-spectrum* $F(\omega)$. However, in this case, $d(\mathbf{a}/3)$, $d(\mathbf{a}/5)$, $d(\mathbf{a}/7)\cdots$ are also found to values of 0. The x values at which $d(x)=0$ can be represented by

$$x_n=\mathbf{a}/(2n+1) \qquad (n=0,1,2,3\cdots), \quad (7)$$

and $S_n(\omega)$ corresponding to the x_n values can be expressed by

$$S_n(\omega)=\sum_{i=-n}^{n}(-1)^{i+n}F(\omega-ix_n). \quad (8)$$

These x values (except for $n=0$) are not hfccs but are recognized as false hfccs. Therefore, the x values leading to $d(x)=0$ consist not only of the true hfccs but also of many false hfccs. If a number of hfccs are involved in an ESR spectrum, it is impossible to select the true values from the infinite number of these x values.

Finally, we discriminated the true hfccs from the false ones. An index function defined by Eq. 9 was found to be the best for this purpose:

$$I_2(x)\equiv\left[\frac{\int_{-\infty}^{\infty}|R(\omega)-R(\omega-\delta)|\,d\omega}{\sum_{j=1}^{2}\int_{-\infty}^{\infty}|R(\omega)-S(\omega-x/2)-S(\omega+x/2+(-1)^j\delta)|\,d\omega}\right]^2, \quad (9)$$

where δ is a very small value. It is replaced by 1 or 2 in actual calculations, which is sufficiently small when compared to N. The subscript in $I_2(x)$ indicates the multiplicity of the nuclear spin of $I=1/2$, namely, $2I+1=2$. The numerator of $I_2(x)$ is used for normalization. Squaring the bracket in this equation is performed for an enhancement of the resolution. Since the denominator of $I_2(x)$ is one of the error functions, such as $d(x)$, it also approaches 0, namely, $I_2(x)$ gives a maximum value when x is equal to **a**. From Eqs. 1, 7, 8, and 9, $I_2(\mathbf{a})$ can be represented by

$$I_2(\mathbf{a})=\left[\frac{\int_{-\infty}^{\infty}|F'(\omega+\mathbf{a}/2)+F'(\omega-\mathbf{a}/2)|\,d\omega}{2\int_{-\infty}^{\infty}|F'(\omega+\mathbf{a}/2)|\,d\omega}\right]^2, \quad (10)$$

where $F'(\omega)$ represents $[F(\omega)-F(\omega+\delta)]/\delta$ or $[F(\omega)-F(\omega-\delta)]/\delta$, which is a form of the derivative of $F(\omega)$. If each line in $F'(\omega+\mathbf{a}/2)+F'(\omega-\mathbf{a}/2)$, that is, in the spectrum obtained from the differentiation of $R(\omega)$, is well resolved and there is no overlap between $F'(\omega+\mathbf{a}/2)$ and $F'(\omega-\mathbf{a}/2)$, the numerator of Eq. 10 can be approximately represented by Eq. 11. Hence, $I_2(\mathbf{a})$ is nearly equal to unity.

$$\begin{aligned}
\int_{-\infty}^{\infty}|F'(\omega+\mathbf{a}/2)+F'(\omega-\mathbf{a}/2)|\,d\omega &\approx\int_{-\infty}^{\infty}|F'(\omega+\mathbf{a}/2)|\,d\omega\\
&+\int_{-\infty}^{\infty}|F'(\omega-\mathbf{a}/2)|\,d\omega=2\int_{-\infty}^{\infty}|F'(\omega)|\,d\omega.
\end{aligned} \quad (11)$$

Since the lines in most of the observed ESR spectra are more or less overlapped, $I_2(\mathbf{a})$ is usually smaller than unity. However, it should be pointed out that the line shape in the ESR spectrum, $R(\omega)$, was not specified in this analysis. If one analyzes the differentiated ESR spectrum, i.e., the 2nd or 3rd derivatives, $I_2(\mathbf{a})$ increases and shows a value closer to unity because the separation of each line becomes better. This distinctive feature is very useful, especially in the analysis of poorly resolved ESR spectra.

If the large second-order effects contribute in the ESR spectra the intensity of $I_2(\mathbf{a})$ will decrease since the basic assumption of NDA, represented by Eq. 1, is not fulfilled.

To discuss the relative intensities of the false and true peaks, the ratio $I_2(\mathbf{a}/3)/I_2(\mathbf{a})$ represented by Eq. 12 is derived from Eqs. 1,7,8, and 9:

$$\frac{I_2(\mathbf{a}/3)}{I_2(\mathbf{a})}=\left[\frac{\int_{-\infty}^{\infty}|F'(\omega+\mathbf{a}/2)|d\omega}{\int_{-\infty}^{\infty}|F'(\omega+\mathbf{a}/2)-F'(\omega+\mathbf{a}/6)+F'(\omega-\mathbf{a}/6)|d\omega}\right]^2,$$

$$=\left[\frac{\int_{-\infty}^{\infty}|F'(\omega)|d\omega}{\int_{-\infty}^{\infty}|F'(\omega+\mathbf{a}/3)-F'(\omega)+F'(\omega-\mathbf{a}/3)|d\omega}\right]^2 \quad (12)$$

The results described in the Appendix indicate that this ratio changes between 1/9 to 1, depending on the degree of overlap of the following three functions: $F'(\omega+\mathbf{a}/3)$, $F'(\omega)$, and $F'(\omega-\mathbf{a}/3)$. When the overlap is small, in other words, the ESR spectrum is well resolved, the intensity of $I_2(\mathbf{a}/3)$ is only one-ninth that of $I_2(\mathbf{a})$. $I_2(\mathbf{a}/3)$ increases with decreasing the resolution of the spectrum, but is still less than $I_2(\mathbf{a})$, even in the worst case. Therefore, $I_2(\mathbf{a}/3)$ is always less than $I_2(\mathbf{a})$. In a similar way, other false hfccs appearing at $\mathbf{a}/5$, $\mathbf{a}/7$,$\cdots$ are found to be much less than $I_2(\mathbf{a})$.

The reason why these false hfccs can be distinguished by the index function $I_2(x)$ is explained as follows: Though $S_1(\omega)$ represented by Eq. 8 is quite different from the real *sub-spectrum* $F(\omega)$, $S_1(\omega+\mathbf{a}/6)+S_1(\omega-\mathbf{a}/6)$ becomes identical to $R(\omega)$ due to a partial canceling between $S_1(\omega+\mathbf{a}/6)$ and $S_1(\omega-\mathbf{a}/6)$ (Fig. 1b). This suggests that these false hfccs can not be distinguished from real values by simply using the error function $d(x)$. However, the index function $I_2(\mathbf{a})$ contains a small distortion of δ which interferes with the canceling, as illustrated in Fig. 2b. Therefore, false values can readily be eliminated by this index function.

Thus, the hfccs contributing to $R(\omega)$ can be readily determined by inspecting the peaks near to unity in a plot of $I_2(x)$ against x.

Numerical Decoupling Analysis for Nuclei with I=1. In the case of a nucleus of I=1, Eqs. 1 and 5 can be substituted by Eqs. 13 and 14, respectively:

$$R(\omega)=F(\omega+\mathbf{a})+F(\omega)+F(\omega-\mathbf{a}), \quad (13)$$

$$\begin{aligned}&S(1)+2S(1+x)+3S(1+2x)+2S(1+3x)+S(1+4x)\\&\quad=R(1+x)+R(1+2x)+R(1+3x)\\&S(2)+2S(2+x)+3S(2+2x)+2S(2+3x)+S(2+4x)\\&\quad=R(2+x)+R(2+2x)+R(2+3x)\\&\quad\vdots\\&S(N-4x)+2S(N-3x)+3S(N-2x)+2S(N-x)+S(N)\\&\quad=R(N-3x)+R(N-2x)+R(N-x).\end{aligned} \quad (14)$$

Some false hfccs appear at

$$x_n=\mathbf{a}/(3n+1)\ (n=1,2,\cdots), \quad (15)$$

or

$$x_m=\mathbf{a}/(3m+2)\ (m=0,1,2,\cdots). \quad (16)$$

S_n and S_m corresponding to x_n and x_m, respectively, can be represented by

$$S_n=\sum_{i=-3n}^{3n} c\,(|i|)\cdot F(\omega-ix_n), \quad (17)$$

and

$$S_m=\sum_{i=-3m-1}^{3m+1} c\,(|i|+2)\cdot F(\omega-ix_m), \quad (18)$$

where

$$\begin{aligned}c(k)&=1 \quad k=3p\\&=0 \quad k=3p+1\\&=-1 \quad k=3p+2,\ p=0,1,2,\cdots.\end{aligned} \quad (19)$$

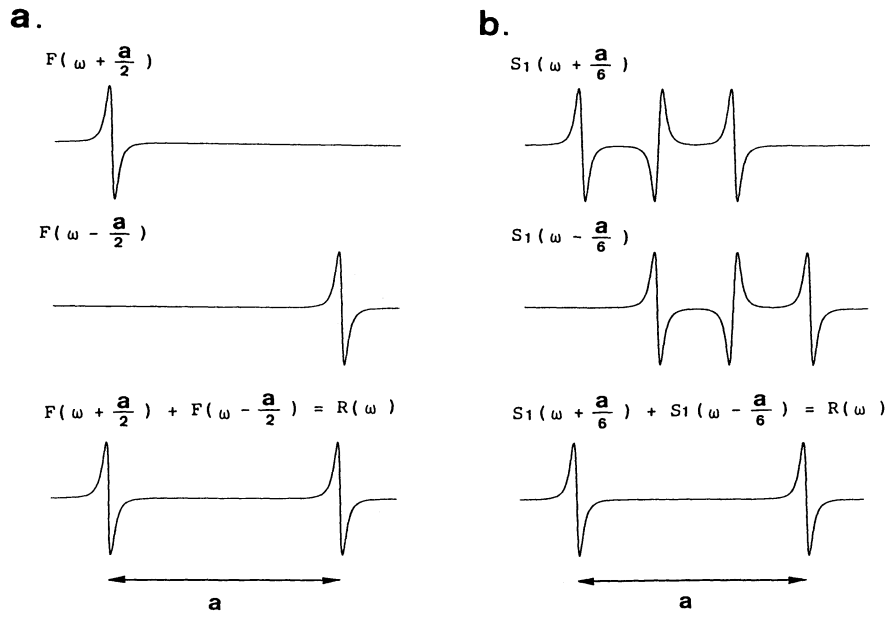

Fig. 1. The illustration of the relationship between the *sub-spectra* and the original ESR spectra (a) at the real hfcc of **a** and (b) at **a**/3, one of the false hfccs.

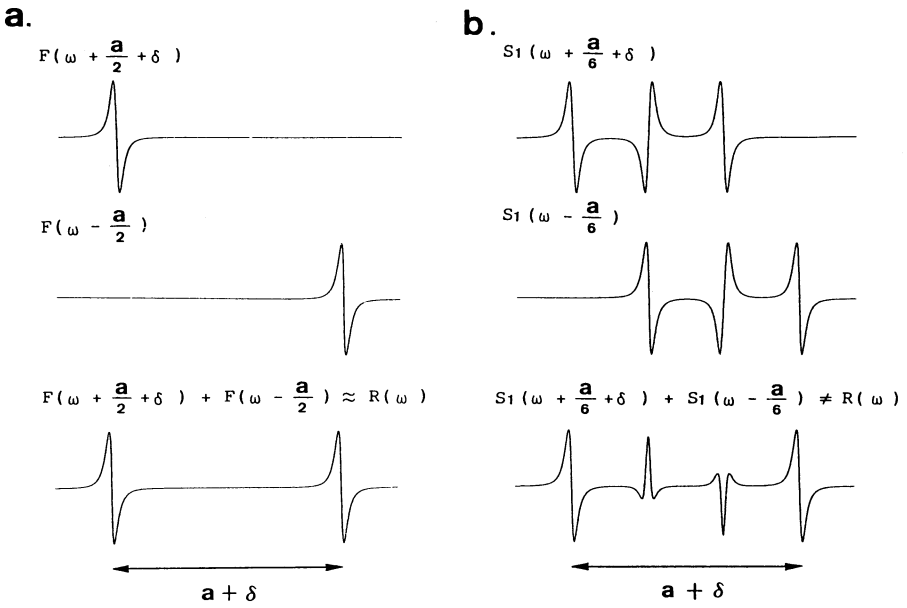

Fig. 2. An illustration showing why false hfccs can be distinguished from the real hfcc by introducing the small distortion δ. (a) The synthesized spectrum from $F(\omega)$ is almost same as the original, $R(\omega)$. (b) The synthesized spectrum from $S_1(\omega)$ is quite different from $R(\omega)$.

The index function for $I=1$ is defined by Eq. 20:

$$I_3(x)=\left[\frac{2\int_{-\infty}^{\infty}|R(\omega)-R(\omega-\delta)|d\omega}{3\sum_{j=1}^{2}\int_{-\infty}^{\infty}|R(\omega)-S(\omega+x)-S(\omega+(-1)^j\delta)-S(\omega-x)|d\omega}\right]^2 \quad (20)$$

In a similar manner as with $I=1/2$, one can show that a plot of $I_3(x)$ against x also gives a maximum value close to unity at $x=\mathbf{a}$.

The ratio $I_3(\mathbf{a}/2)/I_3(\mathbf{a})$ can be represented by

$$\frac{I_3(\mathbf{a}/2)}{I_3(\mathbf{a})}=\left[\frac{\int_{-\infty}^{\infty}|F'(\omega)|d\omega}{\int_{-\infty}^{\infty}|F'(\omega+\mathbf{a}/2)-F'(\omega)+F'(\omega-\mathbf{a}/2)|d\omega}\right]^2 \quad (21)$$

From the results described in the Appendix, the ratio is also found to change between 1/9 to 1, depending on the degree of overlap of the following three functions: $F'(\omega+\mathbf{a}/2)$, $F'(\omega)$, and $F'(\omega-\mathbf{a}/2)$. Therefore, the hfccs of nuclei with $I=1$ can be obtained from a plot of $I_3(x)$ against x in the same way as with $I=1/2$.

Experimental

The preparation of *t*-butyl 4-nitrophenyl nitroxide radical was as follows: 4-nitrophenyl radical produced by the reduction of 4-nitrobenzenediazonium salt with iodide in acetonitrile was trapped by 2-methyl-2-nitrosopropane. After evaporation of the solvent, the nitoxide radical obtained as a spin adduct was separated and purified on a silica-gel column using benzene as an eluent. *t*-Butyl 2-chlorophenyl nitroxide radical was prepared from 2-chlorobenzenediazonium salt in a similar way.

Before ESR measurements benzene solutions of nitroxide radicals in sample tubes were carefully deoxygenated by nitrogen gas bubbling and by several freeze-pump-thaw cycles.

ESR spectra were measured using a JEOL PE-3E, X band ESR spectrometer. ESR spectra were digitized using a 16bit A/D converter (Nippon Protec, Co., Ltd.) of which the acquisition time was 78 ms.

Numerical analyses and calculations of ESR spectra were performed on a PC9801 VX2 micro-computer equipped with a 80286 CPU, and a 80287 co-processor, at a CPU clock cycle of 10 MHz (NEC). Data of a calculated ESR spectrum comprised 1500 points and those of an observed ESR spectrum comprised 1500—2500 points after appropriate treatments, such as digital filtering, centering, and corrections of the offset of the amplifier. These programs for the spectrum treatment, NDA and the calculation of ESR spectra were written in FORTRAN 77. The required computing time for the $I_2(x)$ plot was about 5 minutes and that of the $I_3(x)$ plot was about 10 minutes.

Results and Discussion

Discrimination of the Nuclear Spin of I=1/2 and 1. The plots of $I_2(x)$ in Fig. 3b and $I_3(x)$ in Fig. 3c were obtained for the calculated ESR spectrum (Fig. 3a) from the parameters of $I=1/2$, hfcc=0.06 and a linewidth=0.01 mT. A Lorentzian line shape function was used to obtain all of the calculated spectra in this work. In the $I_2(x)$ plot (Fig. 3b), one well-defined peak of unity height appeared at 0.06 mT. Several additional peaks also appeared at 0.02, 0.012 mT, etc., which were assigned to be false peaks. The ratio

$I_2(\mathbf{a}/3)/I_2(\mathbf{a})$ was calculated to be 0.17, slightly larger than the lowest value predicted by Eq. 12, i.e., 1/9=0.11, since the two lines in the ESR spectrum in Fig. 3a slightly overlapped. However, $I_2(\mathbf{a}/3)$ is still considerably less than $I_2(\mathbf{a})$.

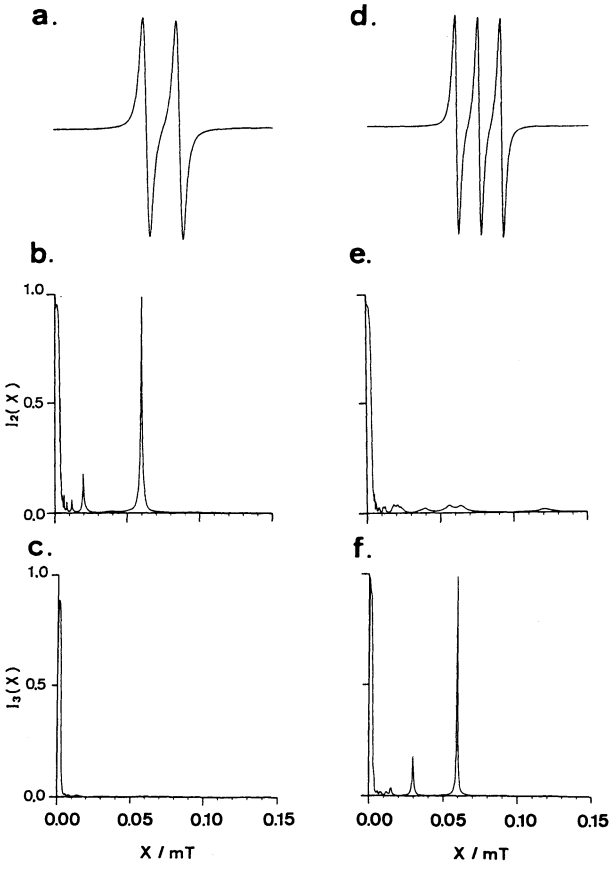

Fig. 3. (a) Simple ESR spectrum calculated using I=1/2, hfcc=0.06 and linewidth=0.01 mT. (b) The $I_2(x)$ plot and (c) $I_3(x)$ plot for the spectrum (a) calculated with δ=1. (d) Simple ESR spectrum; I=1, hfcc=0.06, linewidth=0.01 mT. (e) The $I_2(x)$ plot and (f) $I_3(x)$ plot for the spectrum (d) with δ=1.

A peak with nearly unity height appeared at 0 mT because it was regarded as a hfcc in NDA. This peak is also attributed to the overlap of an infinite number of false peaks. The singularity very near to 0 mT can not be considered as hfcc since it appears at an x value much less than the linewidth (0.01 mT). On the other hand, it is of particular interest to note that the $I_3(x)$ plot (Fig. 3c) did not show any peaks, except that at 0 mT.

Figures 3e and 3f show $I_2(x)$ and $I_3(x)$ plots for the calculated ESR spectrum (Fig. 3d) with I=1, hfcc=0.06 and linewidth=0.02 mT. In the $I_3(x)$ plot, one well-defined peak of unity height appeared at 0.06 mT and several false peaks at 0.03 and 0.015 mT, etc. The ratio $I_3(\mathbf{a}/2)/I_3(\mathbf{a})$ was also evaluated to be 0.17. No peak appeared, except at 0 mT in the $I_2(x)$ plot in this case also.

As indicated by these results, both the nuclear spin and each hfcc involved in an ESR spectrum are readily determined by NDA without interference by any false peaks.

Determination of Small hfcc. The ESR spectra shown in Figs. 4a and 4b were calculated from the hfcc value of 0.06 (5H) and linewidths of 0.02 and 0.05 mT, respectively. When the hfcc was larger than the linewidth, it was readily determined from the position of the peak appearing in the $I_2(x)$ plots (Figs. 4a′ and 4b′). When the linewidth became 0.06 mT, which is the same as the hfcc, the hfs almost disappeared (Fig. 4c) and, hence, it was difficult to determine the hfcc from the ESR spectrum. Even in such a case, one broad peak appeared in the $I_2(x)$ plot (Fig. 4c′), while its peak position shifted slightly to a smaller hfcc value. The accuracy in determining the hfccs by NDA will be discussed later.

Since the line shape is not specified in this analysis, a 2nd-derivative spectrum can also be analyzed. One

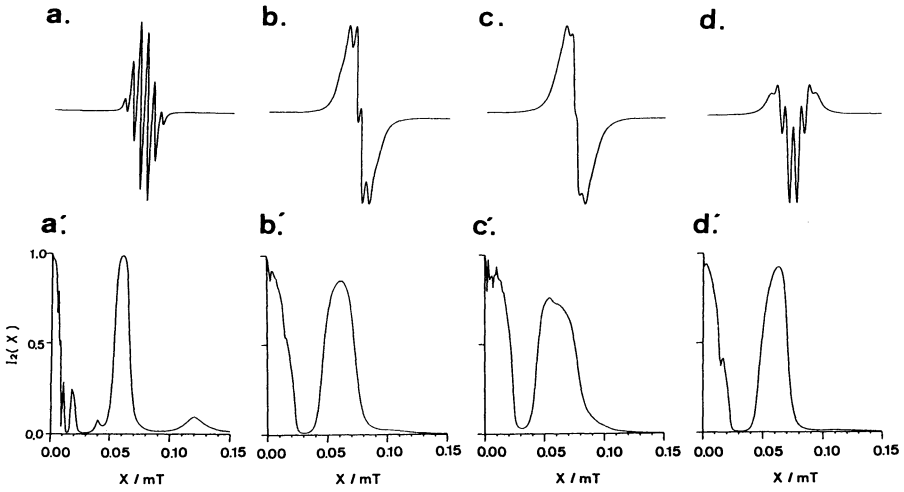

Fig. 4. ESR spectra calculated with hfcc=0.06 mT (5H) and various linewidths of (a) 0.02 (b) 0.05 (c) 0.06 and (d) 0.06 mT (2nd-derivative). (a′), (b′), (c′), and (d′) are respective $I_2(x)$ plots which were obtained with δ=1.

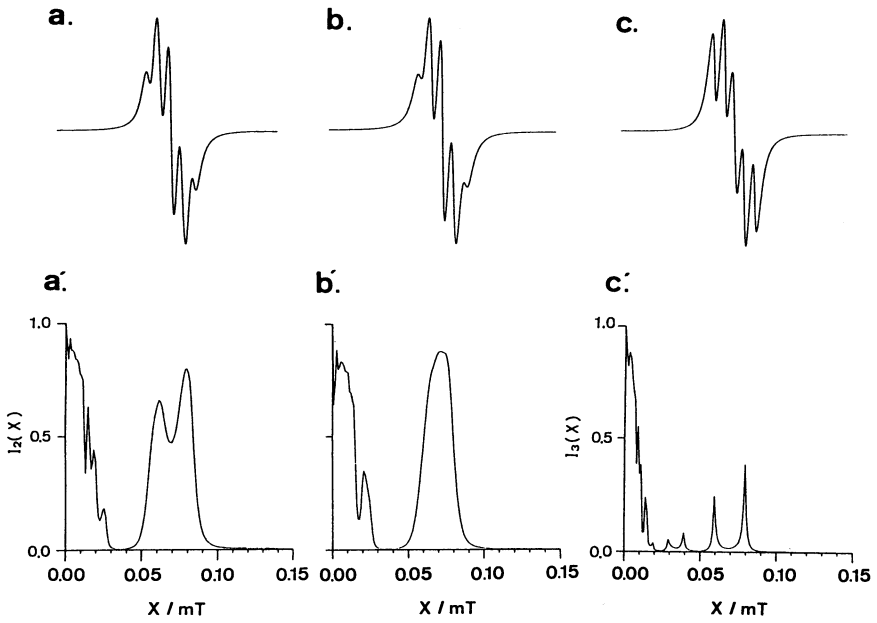

Fig. 5. (a) Calculated ESR spectrum; hfccs=0.06 (2H), 0.08 (2H), linewidth=0.04 mT. (b) hfcc=0.07 (4H), linewidth=0.045 mT. (c) hfccs=0.06 (1N), 0.08 (1N), linewidth=0.04 mT. (a′) and (b′) are the $I_2(x)$ plots for (a) and (b) with δ=1. (c′) was the $I_3(x)$ plot for (c) with δ=1.

sharp peak appeared at 0.06 mT in the $I_2(x)$ plot (Fig. 4d′) for the 2nd-derivative spectrum (Fig. 4d) obtained by differentiating the ESR spectrum in Fig. 4c. Thus, the application of NDA to a higher derivative spectrum permits one to determine accurate hfccs involved in poorly resolved ESR spectra.

The lower limit of the hfcc values for I=1 was also found to be almost the same as for I=1/2 when the first-derivative ESR spectra were analyzed with NDA.

Resolution for Small Difference between hfccs. Next, the resolution for small differences between hfccs was demonstrated. Figure 5a shows the ESR spectrum calculated with a hfcc of 0.06 (2H) and 0.08 (2H), and a linewidth of 0.04 mT. Though the linewidth was twice as large as the difference between the two hfccs, they were completely separated in the $I_2(x)$ plot (Fig. 5a′). On the other hand, this ESR spectrum closely resembled that calculated with hfcc of 0.07 mT (4H) (Fig. 5b). Thus, the hfcc of 0.07 mT would be accidentally obtained if the ESR spectrum in Fig. 5a is analyzed with ordinary methods. It is, however, very interesting to note that the $I_2(x)$ plots shown in Figs. 5a′ and 5b′ obtained for the ESR spectra in Figs. 5a and 5b, respectively, were quite different.

Figure 5c shows an $I_3(x)$ plot for the ESR spectrum calculated from hfccs of 0.06 (1N) and 0.08 (1N), and a linewidth of 0.04 mT. Though two peaks at 0.06 and 0.08 mT were fairly small, they were well resolved.

Effect of Equivalent Nuclei and Delta. Figures 6a and 6d show the ESR spectra calculated from the hfccs of 0.07 (1H) and 0.02 (10H), and linewidth of 0.005 and 0.015 mT, respectively. Figure. 6b shows the $I_2(x)$ plot obtained for the spectrum in Fig. 6a when

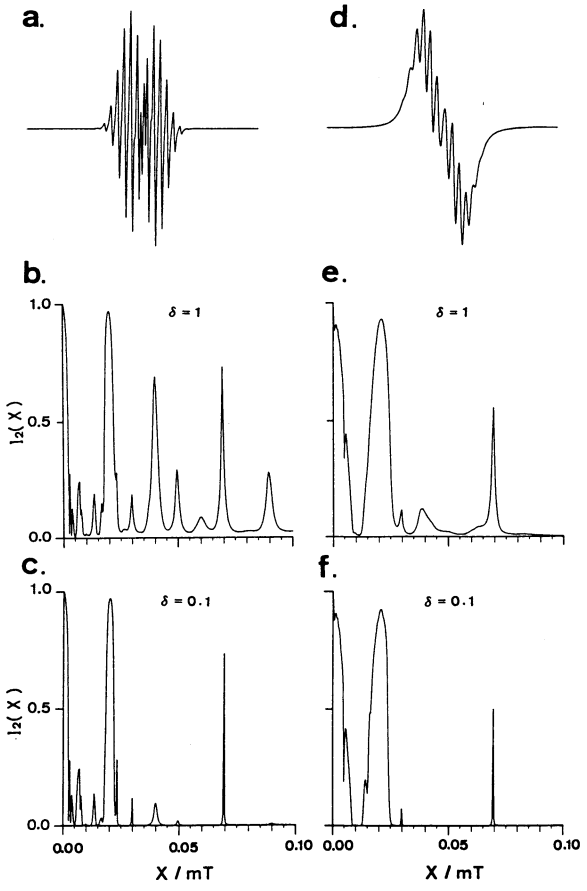

Fig. 6. (a) Calculated ESR spectrum; hfccs=0.02 (10H), 0.07 (1H), linewidth=0.005 mT. (b) The $I_2(x)$ plot for (a) with δ=1 and (c) with δ=0.1. (d) Calculated ESR spectrum with the same parameters as (a) except for a linewidth of 0.015 mT. (e) The $I_2(x)$ plot for (d) with δ=1, and (f) with δ=0.1.

δ=1, which was equal to 0.00035 mT in this calculation. Several peaks appeared in the $I_2(x)$ plot in addition to the hfcc peaks (at 0.02, 0.07 mT) and their false peaks (at 0.014, 0.007 mT). The peaks, which appeared at 0.05 and 0.09 mT, corresponded to 0.07—0.02 and 0.07+0.02 mT, respectively. Those at 0.04 and 0.06 mT seemed to be overtone peaks corresponding to 2×0.02 and 3×0.02 mT, respectively. We call these peaks *sub-peaks*, which differ from false peaks. They sometimes appear when many equivalent nuclei contribute to the hfs. On the other hand, when the linewidth was 0.015 mT, these *sub-peaks* were very small (Fig. 6e), while the hfcc peaks at 0.02 and 0.07 mT were substantially unchanged.

These results indicate that the intensities of the *sub-peaks* are closely related to the ratio of δ to the linewidth. The intensities of the *sub-peaks* increased when the value of δ was not small compared with the linewidth. To suppress the *sub-peaks*, the δ value should be chosen to be less than about 1/40 of the linewidth. Consequently, if the δ value is equal to the sampling interval of the data, each line in an observed ESR spectrum must be composed of more than 100 data points. However, when an observed ESR spectrum includes many lines this condition may be difficult to achieve on a micro-computer with limited memory space and, hence, *sub-peaks* will prohibit obtaining the exact parameters.

In order to calculate Eq. 9 for a δ value less than 1 the following approximations are used:

$$R(\omega-\delta)\approx R(\omega)-[R(\omega)-R(\omega-1)]\delta, \quad (22)$$

and

$$S(\omega\pm\delta)\approx S(\omega)-[S(\omega)-S(\omega\pm1)]\delta. \quad (23)$$

Substitution of Eqs. 22, 23 into Eq. 9 yields Eq. 24.

$$I_2(x)=\left[\frac{\delta\int_{-\infty}^{\infty}|R(\omega)-R(\omega-1)|\,d\omega}{\sum_{j=1}^{2}\int_{-\infty}^{\infty}|R(\omega)-S(\omega-x/2)-S(\omega+x/2)(1-\delta)-S(\omega+x/2+(-1)^j)\delta|\,d\omega}\right]^2. \quad (24)$$

Figures 6c and 6f show $I_2(x)$ plots calculated from Eq. 24 when δ=0.1. The heights of the *sub-peaks* decreased dramatically and the two hfccs of 0.02 and 0.07 mT were readily determined without any ambiguity. It was also realized that the linewidths of the peaks in the $I_2(x)$ plot obtained from the δ value of 0.1 were narrower than those for δ=1. The linewidths of the peaks in $I_2(x)$ and $I_3(x)$ plots seem to depend on the following factors: the linewidth of an ESR spectrum, the number of nuclei, the nuclear spin, and the δ value. The detailed relationship between them is not presently understood.

Effect of Noise. The value of the numerator in Eq. 10, which is equal to $\delta\int_{-\infty}^{\infty}|R(\omega)-R(\omega-\delta)|d\omega$, increases as the noise in $R(\omega)$ increases. In particular, it is greatly affected by the noise of which frequencies higher than those of the signals in $R(\omega)$. Although the value of the denominator in Eq. 10 also becomes large with increasing noise, it may be larger than that of the numerator since the signal-to-noise ratio in the *sub-spectrum* is always worse than that of the original

Table 1. Hfcc Detected by NDA at Various Linewidths

		Linewidth/mT						
		0.1	0.5	1.0	2.0	3.0	4.0	5.0
I=1/2, N=1, hfcc=1.00 mT								
$I_2(x)$	δ=1	1.0000	1.00	1.00	1.00	1.00	1.00	1.00
	δ=0.1	1.0000	1.00	1.00	1.00	1.00	1.00	1.00
$d(x)$		1.0000	1.00	1.00	1.00	1.00	1.00	1.00
mT/point		0.0025	0.01	0.01	0.01	0.01	0.02	0.02
I=1/2, N=4, hfcc=1.00 mT								
$I_2(x)$	δ=1	1.000	1.02	0.94	0.84	0.96		
	δ=0.1	1.000	1.00	1.00	1.00	1.00		
$d(x)$		0.995	1.00	1.00	1.00	1.00		
mT/point		0.005	0.01	0.02	0.02	0.02		
I=1, N=1, hfcc=1.00 mT								
$I_3(x)$	δ=1	1.000	1.00	1.00	1.00	0.88		
	δ=0.1	1.000	1.00	1.00	1.00	0.88		
$d(x)$		1.000	1.00	1.00	1.00	0.88		
mT/point		0.005	0.01	0.01	0.02	0.02		
I=1 ,N=3, hfcc=1.00 mT								
$I_3(x)$	δ=1	1.00	1.01	0.98	0.88			
	δ=0.1	1.00	1.00	0.98	0.88			
$d(x)$		1.00	1.00	0.98	0.88			
mT/point		0.01	0.01	0.02	0.02			

ESR spectrum. Therefore, the value of I_2(**a**) decreases with increasing noise in the original ESR spectrum. In order to avoid this problem it is advisable that a noisy ESR spectrum is treated with a smoothing filter before being examined by NDA.

Accuracy of hfcc Determined by NDA. Hfcc values determined by NDA from the calculated ESR spectra with hfcc=1.00 mT and various linewidths are given in Table 1. The 1st-derivative Lorentzian function was used in the calculation of all the ESR spectra. Table 1 also contains the values determined from the positions of minima of the error function, $d(x)$ (Eq. 4). In the cases of ESR spectra with a nucleus of I=1/2, the hfcc at 1.00 mT could be determined even at a linewidth of 5.0 mT, whereas a hfcc as small as the linewidth may be the smallest which can be determined by NDA in an actual ESR spectrum containing some noise and distortions. As described in the previous section, hfcc smaller than the linewidth can be determined with the aid of numerical differentiation. However, it must be considered that the calculation of a higher derivative of an observed ESR spectrum usually increases the noise, which leads to a decrease in the intensities of the hfcc peaks in the $I(x)$ plot.

It should be pointed out that when linewidths are large, the hfccs values obtained from the $I_2(x)$ plots with δ=1 become less accurate with increasing number of equivalent nuclei, or probably with increasing number of lines in the hfs. However, hfcc values could be accurately determined either from an $I_2(x)$ plot with δ=0.1 or from $d(x)$. Therefore, exact hfccs should be determined either from the index function $I(x)$ calculated with a smaller δ value or from minima of the error function $d(x)$, especially in interpreting poorly resolved ESR spectra.

When the ESR spectra involving the nuclear spin of 1 was examined less accurate values could be obtained, even from $d(x)$ or $I_3(x)$ with δ=0.1 at the larger linewidth (2 and 3 mT). This is because both tails of the ESR spectrum did not decrease to zero and, therefore, the assumption leading to Eq. 6 was not fulfilled.

Analysis of the ESR Spectrum of *t*-Butyl 4-Nitrophenyl Nitroxide Radical. Figure 7a shows the expanded ESR spectrum of the M_I=+1 components due to the nitrogen nucleus of the nitroxide group in *t*-butyl 4-nitrophenyl nitroxide radical (the entire ESR spectrum was depicted in Fig. 7). In the plots of $I_2(x)$ in Fig. 7b and $I_3(x)$ in Fig. 7c one can readily distinguish the hfcc peaks from the false peaks. Values of 0.090 and 0.223 mT as the proton hfcc and 0.0555 mT as the nitrogen hfcc were obtained, though their intensities were less than unity. The peak at 0.074 mT in Fig. 7b is a false peak for 0.223 mT and those at 0.018 and 0.030 mT are false peaks for 0.090 mT.

The simulated spectrum in Fig. 7d using hfccs of 0.090 (2H, *m*), 0.223 (2H, *o*) and 0.0555 mT(1N, NO_2) is in excellent agreement with that of Fig. 7a.

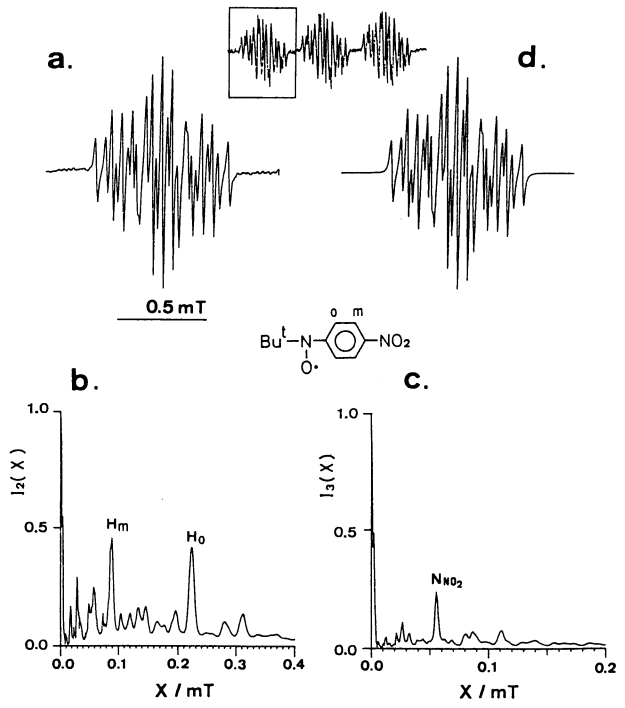

Fig. 7. (a) Expanded ESR spectrum of the M_I=+1 components of *t*-butyl 4-nitrophenyl nitroxide radical (inserted the entire ESR spectrum) measured in a benzene solution. (b) The $I_2(x)$ plot and (c) $I_3(x)$ plot for the spectrum (a) obtained with δ=1. (d) The simulated ESR spectrum using the parameters determined by NDA, i.e., 0.090 (2H, *m*), 0.223 (2H, *o*) and 0.0555 mT (1N, NO_2).

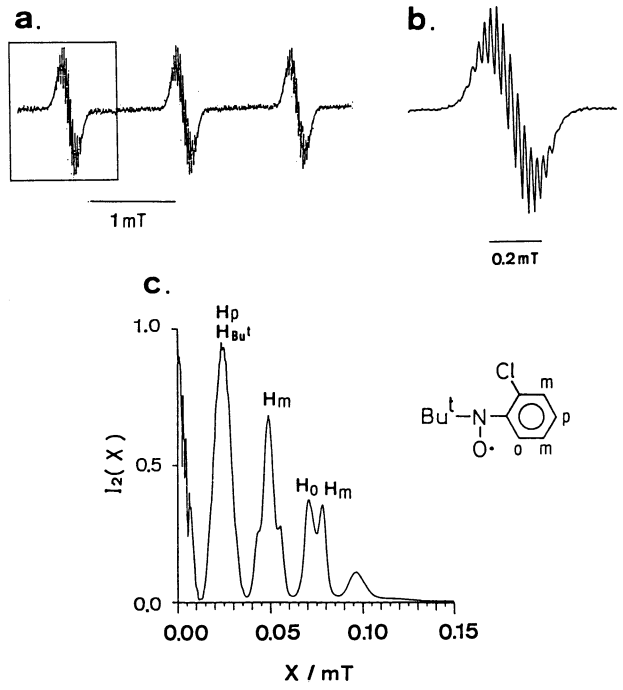

Fig. 8. (a) ESR spectrum of *t*-butyl 2-chlorophenyl nitroxide radical measured in a benzene solution. (b) Expanded spectrum of the M_I=+1 components in (a). (c) The $I_2(x)$ plot for (b) obtained with δ=1.

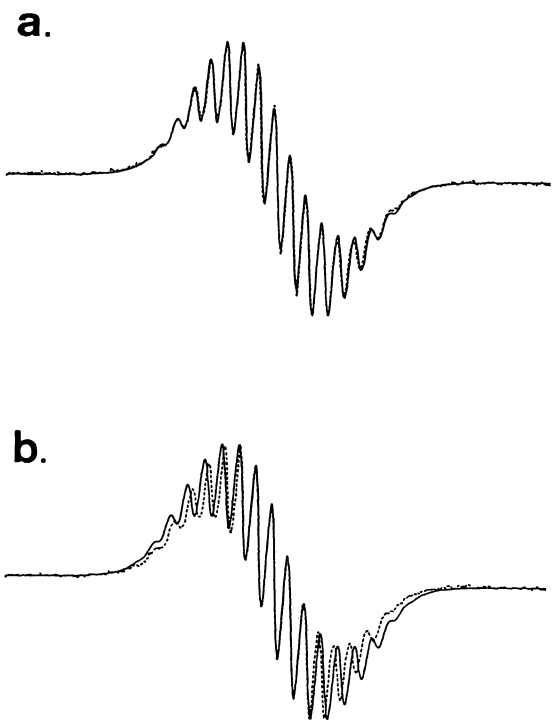

Fig. 9. (a) The simulated spectrum (solid line) using the parameters determined by NDA and (b) using those from NMR data. Experimental ESR spectra were superimposed in both figures with a dotted line (see text).

As indicated here, the nuclear spins and the hfcc values could be obtained from $I_2(x)$ and $I_3(x)$ plots without difficulty, although they were not easily obtained directly from the ESR spectrum (Fig. 7a). Furthermore, since accurate hfccs were determined with the aid of NDA, a computer simulation could be performed only by adjusting the linewidth, and the time for analysis of the ESR spectrum was greatly shortened.

Analysis of the Low-Resolved and Complex ESR Spectrum of *t*-Butyl 2-Chlorophenyl Nitroxide Radical. Figure 8b shows an expanded ESR spectrum of the M_I=+1 components in the ESR spectrum (Fig. 8a) of *t*-butyl 2-chlorophenyl nitroxide radical in benzene. It is obvious that the interpretation of the ESR spectrum is very difficult by ordinary analytical methods since no characteristic pattern appeared in the hfs. It should be noted that four peaks clearly appeared in the $I_2(x)$ plot (Fig. 8c) and, hence, the four hfccs could be precisely determined from these positions. The peak at 0.096 mT, which is nearly equal to 0.024+ 0.0705 mT, seems to be a *sub-peak*. Many peaks appearing in the region from 0 to 0.015 mT could be attributed to the overlap of false peaks for each hfcc. These peaks were excluded because they appear at x values that are much smaller than the linewidth, which is about 0.02 mT in this case.

The ESR spectrum represented by the solid line in Fig. 9a was simulated using hfccs of 0.0240 (10H), 0.0490 (1H), 0.0705 (1H) and 0.0785 (1H), and a linewidth of 0.018 mT. It is in good agreement with the experimental spectrum (superimposed using a dotted line). The hfccs determined by NDA are slightly inconsistent with those obtained from an NMR study of synthesized radicals,[18] which are 0.024 (9H, *t*-butyl), 0.078 (1H, *o*), 0.082 (1H, *m*), 0.049 (1H, *m*), and 0.028 mT (1H, *p*). The small differences between their values and ours can probably be attributed to the large difference in the concentration of radicals ($>$ 1 mol dm^{-3} for NMR and 0.1—1mmol dm^{-3} for ESR observation). These NMR data were obviously inadequate for the analysis of the present ESR spectrum since the simulated spectrum using the NMR data was not in good agreement with the experimental one (Fig. 9b).

These results demonstrate the excellent potentialities of NDA, namely, high resolution for hfcc and an effective elimination of false hfccs.

Conclusion

The general characteristics of NDA can be summarized as follows:

1. One peak in the $I_2(x)$ or $I_3(x)$ plot essentially corresponds to one hfcc.
2. The peak height at the hfcc is nearly equal to unity, but decreases in a poorly resolved ESR spectrum.
3. The height of each hfcc peak does not depend on the number of equivalent nuclei.
4. The nuclear spin can readily be discriminated. For example, nuclei with I=1/2 give peaks in an $I_2(x)$ plot. However, other nuclei, such as nitrogen with I=1, give no peaks.
5. A hfcc as small as a linewidth can be detected.
6. The difference between hfccs as small as about half of the linewidth can be resolved.
7. The line shape in an ESR spectrum is not specified.
8. The δ value used for the calculation of $I(x)$ should be as small as possible, approximately less than 1/30—1/40 of the linewidth. Otherwise, the peak heights of *sub-peaks* usually increase.
9. A noisy ESR spectrum should be treated with a smoothing filter before being examined by NDA.

Among these characteristics, 1, 4, 5, 6, and 7 were better than those of the other numerical methods. In particular, NDA was found to be a valuable tool in analyses of poorly resolved and complex ESR spectra. Since most of these ESR spectra give fewer characteristic patterns in the hfs's, it is very difficult to obtain hfccs from the spectra with ordinary methods. As is demonstrated in Fig. 7, NDA enables one to determine the hfccs exactly, even from spectra showing poorly resolved and monotonous hfs's.

NDA is applicable to the analysis of isotropic ESR spectra with constant linewidths, in which the spectra the basic assumptions represented by Eqs. 1 and 13 are

fulfilled. The deviation from the isotropic spectrum arising, for example, from alternating linewidths, restricted motions, anisotropic interactions, or large second-order effects leads to a decrease of the peak heights in an $I(x)$ plot.

NDA is not a suitable method for analyzing ESR spectra of mixtures of paramagnetic species or those of anisotropic polycrystalline powders.

The well-developed method of electron nuclear double resonance (ENDOR) is better than NDA for the determination of hfccs. However, the ENDOR spectra can be obtained only in limited temperature ranges and, moreover, it costs much more than a micro-computer.

Appendix

Let the areas surrounded by the functions $y=f(\omega+c)$, $y=f(\omega)$ and $y=f(\omega-c)$, and by $y=0$ be $S1$, $S2$, and $S3$, respectively:

$$S1=\int_{-\infty}^{\infty}|f(\omega+c)|\,d\omega, \tag{A-1}$$

$$S2=\int_{-\infty}^{\infty}|f(\omega)|d\omega, \tag{A-2}$$

$$S3=\int_{-\infty}^{\infty}|f(\omega-c)|d\omega. \tag{A-3}$$

Moreover, let the shared area among $S1$, $S2$, and $S3$ be $S123$, and those between $S1$, and $S2$, be $S12$ and between $S2$ and $S3$ be $S23$. Let the unshared areas in $S1$, $S2$, and $S3$ be $S1r$, $S2r$ and $S3r$, respectively.

Using these notations, $S1$, $S2$, and $S3$ can be represented by Eqs. A-4, A-5, and A-6, respectively:

$$S1=S123+S12+S1r, \tag{A-4}$$

$$S2=S123+S12+S23+S2r, \tag{A-5}$$

$$S3=S123+S23+S3r. \tag{A-6}$$

From the relation of $S1=S2=S3$ and Eqs. A-4, A-5, and A-6, one obtains:

$$S1r = S23 + S2r, \tag{A-7}$$

$$S3r = S12 + S2r. \tag{A-8}$$

The denominator of Eq. 12 can be represented by Eq. A-9 by replacing $F'(\omega)$ with $f(\omega)$ and $\mathbf{a}/3$ with c as follows:

$$\begin{aligned}\int_{-\infty}^{\infty}&|F'(\omega+\mathbf{a}/3)-F'(\omega)+F'(\omega-\mathbf{a}/3)|d\omega\\ &=\int_{-\infty}^{\infty}|f(\omega+\mathbf{a}/3)-f(\omega)+f(\omega-\mathbf{a}/3)|d\omega,\\ &=S123+S1r+S2r+S3r.\end{aligned} \tag{A-9}$$

That of Eq. 21 can also be represented by Eq. A-10:

$$\begin{aligned}\int_{-\infty}^{\infty}&|F'(\omega+\mathbf{a}/2)-F'(\omega)+F'(\omega-\mathbf{a}/2)|d\omega\\ &=\int_{-\infty}^{\infty}|f(\omega+\mathbf{a}/2)-f(\omega)+f(\omega-\mathbf{a}/2)|d\omega,\\ &=S123+S1r+S2r+S3r.\end{aligned} \tag{A-10}$$

Substitution of Eqs. A-7 and A-8, and then A-5 into Eq. A-9 yields:

$$\begin{aligned}S123+S1r+S2r+S3r&=S123\\ &+3S2r+S12+S23=S2+2S2r.\end{aligned} \tag{A-11}$$

Since both numerators of Eqs. 12 and 21 are equal to S2, the value of Eqs. 12 and 21 can be represented by

$$\frac{I_2(\mathbf{a}/3)}{I_2(\mathbf{a})}=\frac{I_3(\mathbf{a}/2)}{I_3(\mathbf{a})}=\left[\frac{S2}{S2+2S2r}\right]^2. \tag{A-12}$$

If there is no overlap between $S1$, $S2$ and $S3$, $S2r$ equals $S2$ and the value of Eq. A-12 is 1/9. With increasing the overlap between them, $S2r$ decreases and the value of Eq. A-12 approaches 1:

$$\frac{1}{9}<\left[\frac{S2}{S2+2S2r}\right]^2<1. \tag{A-13}$$

This work was supported in part by a Grant-in-Aid for Scientific Research No. 62540436 from the Ministry of Education, Science and Culture.

Thanks are also due to the Murata Science Foundation for financial assistance.

References

1) D. W. Marquardt, R. G. Bennett, and E. J. Burrell, *J. Mol. Spectrosc.*, **7**, 269 (1961).
2) A. Bauder and R. J. Myers, *J. Mol. Spectrosc.*, **27**, 110 (1968).
3) L. Fischer, *J. Mol. Spectrosc.*, **40**, 414 (1971).
4) M. Barzaghi and M. Simonetta, *J. Magn. Reson.*, **51**, 175 (1983).
5) A. L. J. Beckwith and S. Brumby, *J. Magn. Reson.*, **73**, 252 (1987).
6) B. Kirste, *J. Magn. Reson.*, **73**, 213 (1987).
7) E. Ziegler and E. G. Hoffmann, *Fresenius' Z. Anal. Chem.*, **240**, 145 (1968).
8) K. D. Bieber and T. E. Gough, *J. Magn. Reson.*, **21**, 285 (1976).
9) G. Grampp and C. A. Schiller, *Anal. Chem.*, **53**, 560 (1981).
10) A. Motten and J. Schreiber, *J. Magn. Reson.*, **67**, 42 (1986).
11) D. W. Kirmse, *J. Magn. Reson.*, **11**, 1 (1973).
12) W. R. Dunham, J. A. Fee, L. J. Harding, and H. J. Grande, *J. Magn. Reson.*, **40**, 351 (1980).
13) R. H. Silsbee, *J. Chem. Phys.*, **45**, 1710 (1966).
14) O. Dračka, *J. Magn. Reson.*, **45**, 187 (1985).
15) R. Newton, K. F. Schultz, and R. M. Elofson, *Can. J. Chem.*, **44**, 752 (1966).
16) A. G. Motten, D. R. Duling, and J. Schreiber, *J. Magn. Reson.*, **71**, 34 (1987).
17) K. Lüders, *J. Magn. Reson.*, **73**, 1 (1987).
18) J. A. Pedersen and K. Torssell, *Acta. Chem. Scand.*, **25**, 3151 (1971).